PERGAMON

Journal of Atmospheric and Solar-Terrestrial Physics 63 (2001) 759–770

Journal of ATMOSPHERIC AND SOLAR-TERRESTRIAL PHYSICS

www.elsevier.nl/locate/jastp

Modelling of particle charging in the polar summer mesosphere: Part 1—General results

Markus Rapp, Franz-Josef Lübken *

Leibniz Institut für Atmosphärenphysik, Schlossstr. 6, 18225 Kühlungsborn, Germany

Received 26 February 2000; accepted 22 November 2000

Abstract

Rocketborne measurements of electron and positive ion number densities in the vicinity of noctilucent clouds and/or polar mesosphere summer echoes frequently give evidence of pronounced disturbances relative to a smooth background profile. A model is applied to study the disturbances in terms of diffusional charging of aerosol particles with special regard to the background plasma conditions, i.e. the electron/ion production rate and the coefficient of dissociative recombination which depends on the positive ion composition. It is demonstrated that the disturbances in electron and positive ion profiles are a complex function of the aerosol radius, the aerosol number density, the production rate, and the recombination coefficient. However, if the latter two are known, the model allows the determination of aerosol radii and number densities from the measurement of positive ion and electron number densities. Furthermore, we show that nearly all combinations of electron biteouts, positive ion biteouts, and positive ion enhancements can exist depending on the properties of the aerosol particles and the background plasma conditions. Concerning electrons the presence of aerosol particles will always lead to a depletion. The magnitude of this depletion increases with increasing aerosol size and number density. Concerning positive ions both depletions and enhancements can occur. While small electron/ion production rates favour deep depletions in both electrons and positive ions, enhancements in positive ions are most likely created if the recombination coefficient is large implying large positive cluster ions. However, enhancements of electrons cannot be created by the variation of the above mentioned parameters. Thus observations of electron enhancements are a strong indication of a charging mechanism different from the diffusional charging discussed in this paper, e.g. photo emission. We have applied the charging model to in situ observations of electrons and positive ions in the vicinity of noctilucent clouds and polar mesosphere summer echoes. These results are presented in a companion paper by Lübken and Rapp (J. Atmos. Sol. Terr. Phys. (2001), 63, 771–780).

Keywords: Polar summer mesosphere; Aerosol particles; Charging processes; D-region; PMSE; NLC

1. Introduction

Rocketborne measurements of electron and positive ion number densities in the polar summer mesosphere frequently show pronounced disturbances relative to a smooth background profile between 80 and 90 km. One of the very first example of such disturbances was the measurement of electron densities by a Faraday rotation experiment and positive ion densities by an electrostatic ion probe, both from the same rocket payload (Pedersen et al., 1969). Pedersen reported about a pronounced decrease in the electron density profile at an altitude of 87 km simultaneously with a significant decrease in the current measured by the ion probe. Since these disturbances were measured close to altitudes where usually noctilucent clouds are observed (82–85 km), he speculated about the possibility that aerosol particles could act as a sink for electrons. Noctilucent clouds are thought to consist of water ice crystals which nucleate around the temperature minimum of the summer mesopause on either meteoric dust particles or water cluster ions and

* Corresponding author. Tel.: +49-38293-68100; fax: +49-38293-6850.

E-mail address: luebken@iap-kborn.de (F.-J. Lübken).

1364-6826/01/$ - see front matter
PII: S1364-6826(01)00006-2

then sediment and grow to visible size by condensation and coagulation (Hesstvedt, 1961; Turco et al., 1982). Since no NLCs were observed from the ground during that rocket flight it was argued that subvisible particles with radii on the order of 1–10 nm could have a similar effect as (visible) NLC particles. Since that time these disturbances have frequently been observed inside or above a NLC layer. They have also been observed in the upper summer mesosphere with the confirmed absence of NLCs.

When Ecklund and Balsley (1981) reported about very strong radar echoes from the polar summer mesosphere which were later called polar mesosphere summer echoes (PMSE) it was soon proposed that the echoes are also closely related to these aerosol particles. In the 1990s simultaneous radar and lidar measurements of PMSE and NLC, respectively, showed that NLCs are normally located at the lower edge of the PMSE layer (Nussbaumer et al., 1996; von Zahn and Bremer, 1999) which suggests that PMSEs are related to aerosol particles which are too small to be seen from the ground by lidar or by the naked eye (Kelley et al., 1987; Cho et al., 1992; Klostermeyer, 1997).

In this paper we present a model describing the observed disturbances in the plasma densities. Our model is based on previous work by Jensen and Thomas (1991), who analyzed the aerosol charging processes in terms of diffusional charging by electrons and positive ions and determined the feedback of the charged particles on the background plasma. Extending this model we find that the electron/ion production rate, Q, and the dissociative recombination coefficient between electrons and positive ions, α, play a crucial role when trying to explain the plasma measurements by aerosol charging. The importance of Q has been pointed out previously (Reid, 1997) but no comprehensive analysis of the role of the recombination coefficient α for aerosol charging has been presented so far. We note that α is mainly determined by the positive ion composition (see Section 2.3.2).

With our model we have performed various case studies in order to find out which combinations of aerosol parameters (i.e., number densities and radii) and background plasma conditions (i.e., ionization rates and recombination coefficients) are required to produce depletions ('biteouts') or enhancements in the electron and ion density profile. In Section 2.1 we give a short overview of the procedure we have used to calculate the aerosol charge distributions. We will then consider the feedback of the charged aerosol particles on the background plasma (Section 2.2). Finally, the dependence of this feedback on the electron/ion production rate and the coefficient of dissociative recombination is discussed in Section 2.3.

In a second paper (Lübken and Rapp, 2001) we give an overview of all existing simultaneous measurements of electron and positive ion number densities in the presence of NLC and/or PMSE. We have studied different cases of plasma disturbances which are explained in terms of aerosol charging. These studies finally lead to aerosol parameters (radius and number densities) which are important quantities for our understanding of the microphysical properties of NLC and PMSE particles.

2. The aerosol charging model

2.1. The statistical charge distribution of aerosol particles

Following Parthasarathy (1976) the charge distribution of aerosol particles in an ambient plasma can be described by the following recursion relation:

$$P_q(\nu_p + \nu_q^+ n_i + \nu_q^- n_e) = P_{q+1}\nu_{q+1}^- n_e + P_{q-1}(\nu_{q-1}^+ n_i + \nu_p). \quad (1)$$

Here, $P_q(r)$ represents the number density of particles with fixed radius r_A which have accumulated a number of q charges; ν_p is the photo emission rate; ν_q^+ and ν_q^- are the capture rates of positive ions and electrons by a q-charged aerosol; n_i and n_e are the number densities of positive ions and electrons, respectively. The capture rates depend both on the size and the charge of the particles. To give some typical numbers, the capture rate of an electron by a negatively charged or positively charged aerosol particle with a typical radius of 10 nm in a plasma with $n_e = n_i = 1000\ \mathrm{cm}^{-3}$ is $n_e\nu_{-1}^- = 9.4 \times 10^{-5}$ 1/s, and $n_e\nu_{+1}^- = 3.1 \times 10^{-1}$ 1/s, respectively. For comparison, the photoemission rate from a 10 nm ice particle is $\nu_p = 4.4 \times 10^{-7}$ 1/s. For more details about the capture rates we refer to the comprehensive paper by Natanson (1960) and the recent analysis by Rapp (2000). Details about the calculation of photo emission rates are presented in Rapp and Lübken (1999). Note that we consider electrons, positive ions (mainly NO^+, O_2^+, and $H^+(H_2O)_n$), and charged aerosols to be the only charge carriers at altitudes above 80 km in the 24 h illuminated polar summer D-region. Negative ions can most probably be neglected under daylight conditions at such altitudes since they are efficiently destroyed by photodetachment reactions (Mitra, 1981; Thomas and Bowman, 1985).

The left hand side of Eq. (1) represents all loss mechanisms for q-charged particles (namely photo emission, ion capture and electron capture of a q-charged particle) whereas the right hand side expresses their sources: electron capture of a $(q+1)$-charged particle, and ion capture and photo emission of a $(q-1)$-charged particle. In the current paper we will focus on ice particles for which photo emission can be neglected and we will consider particles with a minimum of -5 negative and $+3$ positive mean charges. [1] Despite the fact that a part of the aerosol ensemble can acquire a positive charge, the net aerosol charge will always be less than or equal to zero due to the high thermal mobility of electrons compared to ions. For a detailed discussion of positively charged particles due to photoelectrical effects we refer to

[1] Note that for numerical stability the actual calculations were performed for an even wider range of negative and positive charges to exclude influences from the boundary conditions.

the analysis by Rapp and Lübken (1999). Furthermore, we will consider monomodal aerosol size distributions only to demonstrate major effects and not to confuse the picture by introducing too many unknowns.

The actual charge distribution for a fixed radius r_A is calculated assuming that P_{-10} is zero. An arbitrary value is then assigned to P_{-9}, and P_{-8} is then caculated from Eq. (1), and so on. Finally, P_q is normalized such that $\sum_q P_q(r_A) = N_A(r_A)$, where $N_A(r)$ is the total number density of aerosols with radius r_A.

2.2. The feedback on the background plasma

The steady state electron and ion number densities are given by the continuity equations (Jensen and Thomas, 1991):

$$\frac{\partial n_e}{\partial t} = Q - \alpha n_e n_i - D^- n_e = 0, \tag{2}$$

$$\frac{\partial n_i}{\partial t} = Q - \alpha n_e n_i - D^+ n_i = 0, \tag{3}$$

Q is the electron/ion production rate, α is the coefficient of dissociative recombination, D^- the loss coefficient of electrons to aerosols, and D^+ the loss coefficient of ions to aerosols, respectively. In our nomenclature the condition of local charge neutrality is given by

$$n_i + Z_A = n_e, \tag{4}$$

where Z_A is the net charge number density of the N_A aerosols:

$$Z_A = \sum_q q \cdot P_q. \tag{5}$$

We start our calculations by assuming that the electron and ion number densities are not disturbed ($n_e = n_i = \sqrt{Q/\alpha}$) and then determine the charge distribution P_q from Eq. (1). The next step is to calculate the loss coefficients $D^{+,-}$ from

$$D^- = \sum_q v_q^- P_q, \tag{6}$$

$$D^+ = \sum_q v_q^+ P_q. \tag{7}$$

The steady state electron and ion number densities can then be computed by inserting D^+ and D^- into Eqs. (2) and (3). Normally this results in values for n_e and n_i which are different from the undisturbed values $\sqrt{Q/\alpha}$. Therefore, the entire sequence (calculating the charge distribution, then the loss coefficients $D^{+,-}$ and then the 'new' values of n_e and n_i) is repeated until convergence in n_e and n_i is achieved, which is usually the case after some iterations.

As will be shown below this model allows to deduce the aerosol particle radius and number density from measurements of electron and positive ion number densities and background plasma parameters (Q and α). By capturing ions and electrons from the background plasma, aerosol particle ensembles leave their 'fingerprints' in the background plasma. In Fig. 1 we show contour lines of relative electron and positive ion disturbances Δn_e and Δn_i as a function of particle number density and particle radius. Δn_e and Δn_i are defined as follows:

$$\Delta n_{e,i} = 100 \cdot \frac{n_{e,i} - N_{e,i}}{N_{e,i}}, \tag{8}$$

where n_e (n_i) is the electron (positive ion) number density in the presence of aerosol particles, and N_e (N_i) $= \sqrt{Q/\alpha}$ are the undisturbed background number densities which would exist if no particles were present. A value of $\Delta n_e = -100\%$ implies that all electrons have been captured by the aerosols, $\Delta n_e = 0\%$ is no disturbance at all, and a positive value stands for a density enhancement. Fig. 1 has been calculated for a recombination coefficient $\alpha = 10^{-6}$ cm^3/s and an electron/ion production rate $Q = 10/(\text{cm}^3\text{s})$ representative for a mixture of proton clusters and molecular ions and normal ionospheric daytime conditions, respectively.

From Fig. 1 a combination of electron and ion number density disturbances, Δn_e and Δn_i, is unambiguously related to a certain aerosol radius and number density. For example, values of $\Delta n_i = 0\%$ and $\Delta n_e = -80\%$ lead to a particle radius of 10 nm and a number density of $\approx 2500/\text{cm}^3$. Another example: $\Delta n_i = -30\%$ and $\Delta n_e = -50\%$ results in an aerosol radius of 40 nm and a number density of $270/\text{cm}^3$. Fig. 1 demonstrates that the information imprinted into the plasma profiles leads to an unambiguous determination of aerosol particle parameters.

There is an additional constraint on the possible combinations of particle radii and number densities given by the fact that the particles consist of water ice and that the total amount of water vapor is limited in the upper atmosphere. The number density of water molecules in the particles is calculated from $n_{H_2O} = N_A \cdot (4\pi/3) r_A^3 \cdot \rho_{H_2O}/m_{H_2O}$ where m_{H_2O} is the mass of a water molecule and ρ_{H_2O} the density of water ice. Following Turco et al. (1982) we have used $\rho_{H_2O} = 0.93$ g/cm^3. The mixing ratio of water vapor is then obtained from $c(H_2O) = n_{H_2O}/n_{air}$, where n_{air} is the number density of air in the upper mesosphere. Typical water vapor mixing ratios in the polar upper mesosphere are expected to be less than $\sim$2.5 ppm$_v$ at 85 km (e.g., Seele and Hartogh, 1999; Garcia and Solomon, 1994). However, the equivalent water vapor content of the aerosol particles could be somewhat larger since the aerosol particles might have scavenged the water vapor molecules over a larger altitude range when sedimenting from the mesopause at 88 km down to typical NLC and PMSE altitudes (82–85 km). This effect is known in the literature as the 'freeze drying' effect (Turco et al., 1982; Inhester et al., 1994).

We will later use a mixing ratio of 10 ppm$_v$ as a reasonable upper limit for the water vapor stored in the particles since such values have been recently reported as a result of 3-color observations of NLC by lidars (von Cossart et al., 1999). We present water vapor mixing ratios as a function of r_A and

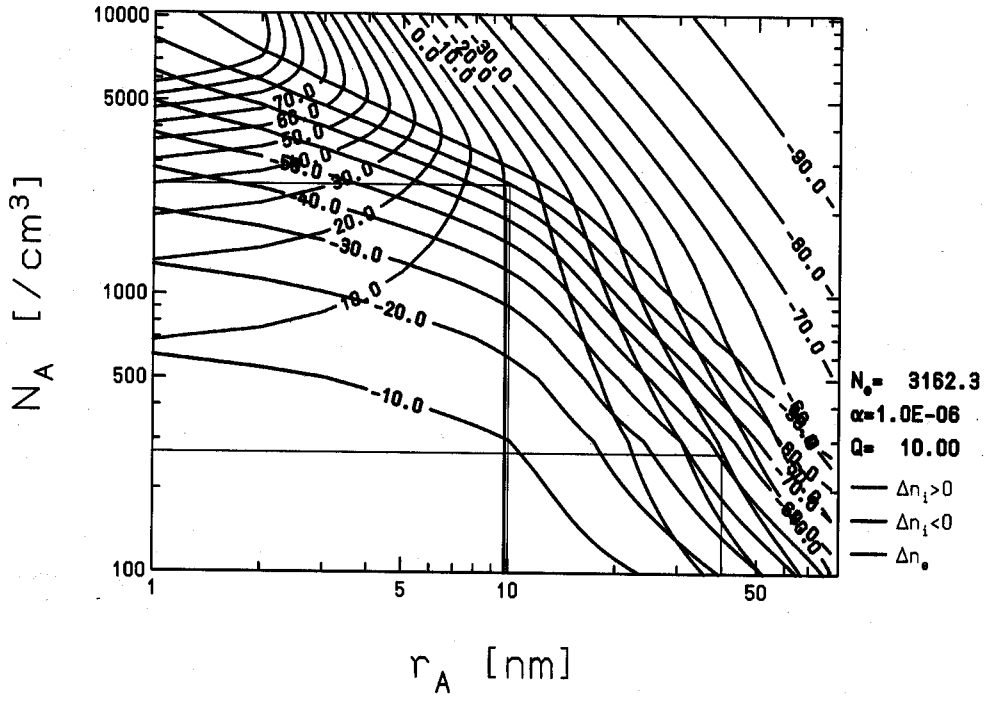

Fig. 1. Relative disturbance of electron (blue lines) and positive ion number density (green and red lines), Δn_e and Δn_i, as a function of the particle radius, r_A, and number density, N_A. The definitions of Δn_e and Δn_i are given in the text. The calculations have been performed for an electron/ion production rate $Q = 10/(\mathrm{cm^3 s})$ and a recombination coefficient $\alpha = 10^{-6}$ cm^3/s.

N_A in Fig. 2 for an altitude of 83 km. Accepting an upper limit of 10 ppm$_v$ being stored in the particles restricts the allowed range of aerosol radii and number densities to the left of the 10 ppm$_v$-line.

2.3. *On the role of background ionization and recombination*

In their model Reid (1990) and Jensen and Thomas (1991) used the same values for the electron/ion production rate and the recombination coefficient, namely $Q = 10/\mathrm{cm^3}$ s and $\alpha = 10^{-6}$ cm^3/s which results in undisturbed electron and ion number densities of $\sim 3100/\mathrm{cm^3}$. These values for Q and α are representative for a mixture of equal numbers of molecular and cluster ions and normal ionospheric daytime conditions at altitudes of about 85 km. Using these numbers the authors found that aerosols with $r_A < 10$ nm are singly negatively charged. If these aerosol particles are numerous enough then they will lead to a distinct biteout in the electron profile leaving the positive ion concentration more or less undisturbed. Later, Reid (1997) pointed out that this result depends on the ionization rate Q. He argued that for very small values of Q (thus small electron and ion number densities) the aerosol particles could capture the entire population of electrons and positive ions leaving a deep biteout in the electron and ion number density profiles. The net charge of the aerosol particles will then be zero since on average the aerosol particles will have captured as many electrons as positive ions.

In the following sections we will investigate in more detail the effect of the ionization rate and the recombination coefficient on the disturbance in the plasma.

2.3.1. *Varying the ionization rates*

What is the natural variability of the ionization rate Q? The variation of Q can be estimated from the variation of observed electron density profiles applying the relation $Q = \alpha \cdot N_e^2$ fixing the recombination coefficient α to a standard value. According to a recent empirical model of Friedrich and Torkar (1995) the daytime electron number density at auroral latitudes can be expressed as a function of the solar zenith angle χ and the riometer absorption L_{rio} characterizing geomagnetic activity:

$$N_e = A + B\left(L_{quiet}\left(\frac{1}{\mathrm{Ch}(\chi)}\right)^{0.4} + L_{rio}\right), \qquad (9)$$

where $L_{quiet} = 0.8$ dB is the background absorption for the hypothetical condition of an overhead sun and $\mathrm{Ch}(\chi)$ is the Chapman function. A and B are coefficients which Friedrich and Torkar (1995) have obtained by fitting Eq. (9) to a large set of radio wave propagation measurements in the polar summer D and E region. For the particular altitude of 85 km they obtain $A = -1.41 \times 10^{-9}/\mathrm{m^3}$ and $B = 1.1 \times 10^{10}/\mathrm{dB\ m^3}$.

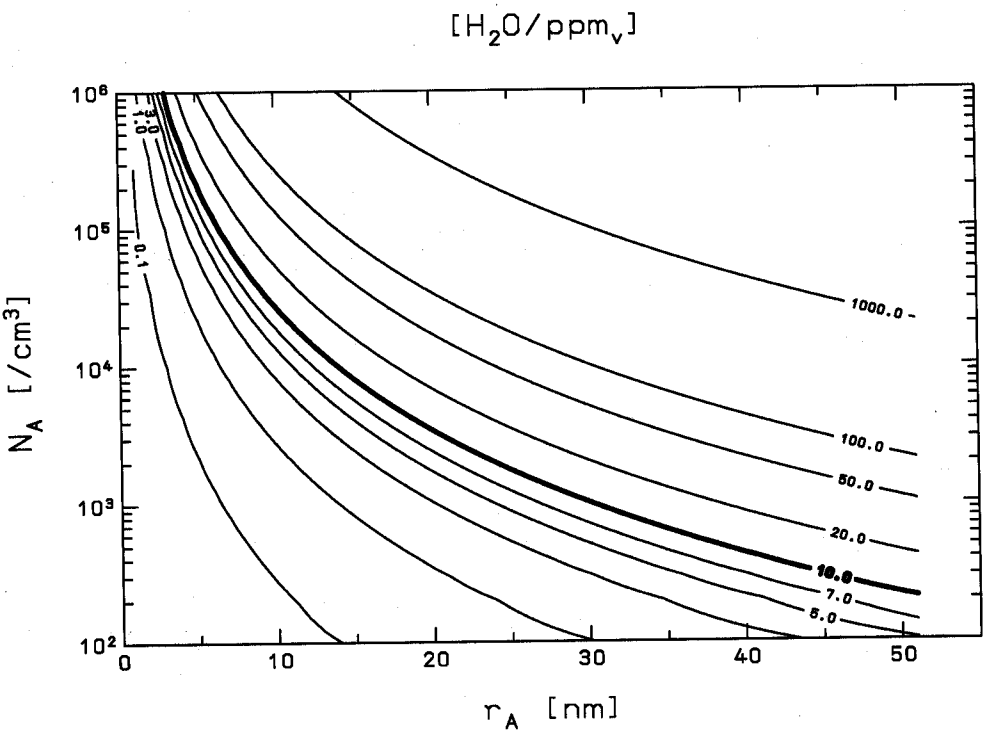

Fig. 2. Contourlines of the water vapor mixing ratio in ppm_v as a function of aerosol particle radius and number density calculated for an altitude of 83 km. A ratio of 10 ppm_v is indicated by a thick solid line.

Using Eq. (9) and $Q = \alpha \cdot N_e^2$ we have calculated the variation of Q as a function of local time for different levels of geomagnetic activity expressed by L_{rio} using a moderate choice for α, i.e. $\alpha = 10^{-6}$ cm^3/s. In the upper panel of Fig. 3 we show the variation of the solar zenith angle χ as a function of local time for August 1 and a geographical latitude of 69°N. From the lower panel we see that for L_{rio}=0 dB (i.e., no particle precipitation) the ionization rate shows a significant variation with local time, thus with χ. While for $\chi \approx 50°$ the electron and ion production rate Q is larger than 10/cm^3 s it drops to values as low as 5×10^{-3}/cm^{3}s for zenith angles larger than 90°. We summarize that the natural variability of Q can be rather large (several orders of magnitude), even more so if we consider the possible range of geomagnetic activity.

How does this variability in Q affect the interaction between the background plasma and the aerosol particles? The important point is that by varying Q and keeping N_A constant the amount of background electrons and ions, i.e. $N_e = N_i = \sqrt{Q/\alpha}$, varies relative to the amount of aerosols. In the upper panel of Fig. 4 we show the mean aerosol charge $\bar{z}_A = Z_A/N_A$ as a function of aerosol radius for various values of N_A/N_e. If free electrons are far more abundant than aerosols ($N_A/N_e \ll 1$) we get results familiar from Jensen and Thomas (1991): For particles smaller than ~10 nm the mean charge is −1e. For larger particles the mean (negative) charge increases linearly with radius. However, the situation changes completely if the aerosol abundance is close to or even larger than the abundance of free electrons. Now the mean particle charge can be much smaller than −1e and the mean charge no longer increases with aerosol radius. If there are far more aerosols in the atmosphere than free electrons ($N_A/N_e \gg 1$) the net charge of the aerosols is zero since all electrons and ions are captured on the aerosols. The effect of decreasing net aerosol charge with increasing N_A/N_e is also clearly seen in the lower panel of Fig. 4. It shows the aerosol charge distribution (normalized to unity) as a function of aerosol charge for aerosol particles with a radius of 8 nm again for different ratios of N_A/N_e. For small ratios of N_A/N_e the charge distribution is narrow and centered at −1e. For larger ratios the distribution becomes broader and the center moves towards zero indicating that the aerosol particle ensemble consists of as many negatively and positively charged particles.

2.3.2. *Varying the recombination coefficient*

As will be explained below the variability of the plasma disturbance by varying the recombination coefficient α is even larger than by varying Q. We note that α is basically determined by the composition of the positive ions. Reid (1990) and Jensen and Thomas (1991) used $\alpha = 10^{-6}$ cm^3/s. Such a recombination coefficient is relevant for an equal

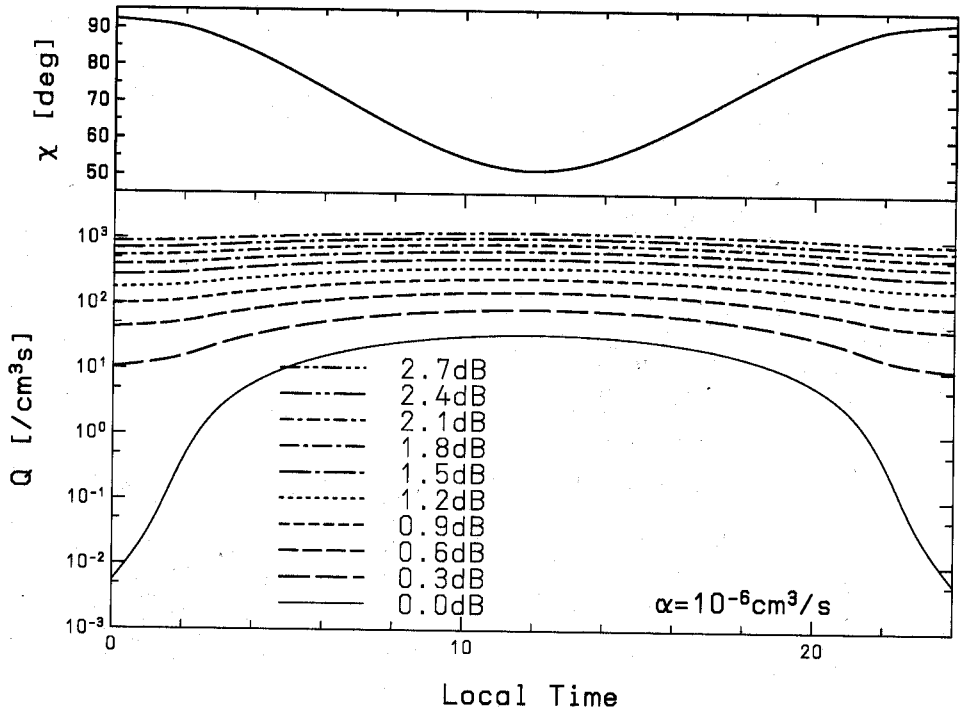

Fig. 3. Upper panel: Variation of the solar zenith angle for August 1 and a geographical latitude of 69°N. Lower panel: Variation of the ionization rate Q as a function of local time for different levels of geomagnetic activity indicated by riometer absorption.

number of proton hydrates and molecular ions which presumably only occurs in a very limited altitude range called the 'transition height'. Above this altitude molecular ions prevail whereas below this height cluster ions are more abundant (Johannessen and Krankowsky, 1972; Kopp et al., 1985). Measurements have shown that this transition altitude can vary significantly, i.e. between 70 and 95 km (Friedrich and Torkar, 1988). This implies a great variability of the composition of positive ion species in the altitude range where mesospheric aerosol layers occur. Indeed, measurements performed with positive ion mass spectrometers in the upper mesosphere have shown that the positive ion composition (thus the recombination coefficient) can vary substantially at these altitudes (Johannessen and Krankowsky, 1972; Kopp et al., 1985).

In Table 1 we have summarized the recombination coefficients for the most important positive molecular ions present in the polar summer mesosphere. As can be seen from this table the recombination coefficient can vary from 10^{-7} cm^3/s for molecular ions like O_2^+ up to values of 10^{-5} cm^3/s for large cluster ions. Note that cluster ions with as much as 21 ligands have been detected in the polar summer D region (Björn and Arnold, 1981). Unfortunately, measurements of the recombination coefficients have been performed for up to 7 ligands only but it is speculated that α further increases for $n > 7$ (Leu et al., 1973) so that recombination coefficients as large as several 10^{-5} cm^3/s could indeed occur. We conclude that the natural variability of α is most probably as large as 2 orders of magnitude in the polar upper mesosphere during summer.

To demonstrate the importance of the recombination coefficient α for modelling the charging processes of mesospheric aerosol particles we have calculated the steady state distributions of electrons, ions, and charged aerosols as a function of α. We have performed these calculations for two different aerosol populations, namely 10 nm size aerosols with a number density of 4000/cm^3, and 50 nm size aerosols with a number density of only 100/cm^3. These populations are usually thought to be representative of PMSE (10 nm) and NLC (50 nm) conditions, respectively (e.g., Reid, 1990; von Cossart et al., 1999). The ionization rate was fixed at 10/cm^{3}s. The results of these calculations are shown in Fig. 5.

In the PMSE case (upper panel in Fig. 5) the electron number density is depleted by more than one order of magnitude, independent of α. The absolute value of the positive ion number density hardly shows any variation with the recombination coefficient. However, by comparing the positive ion number density with the undisturbed background plasma density $\sqrt{Q/\alpha}$, a rather complex pattern is observed: While for $\alpha < 10^{-6}$ cm^3/s the positive ion densities are slightly depleted (e.g. from 10^4/cm^3 to 2500/cm^3 for $\alpha = 10^{-7}$ cm^3/s) the ion densities are even enhanced for larger values of α

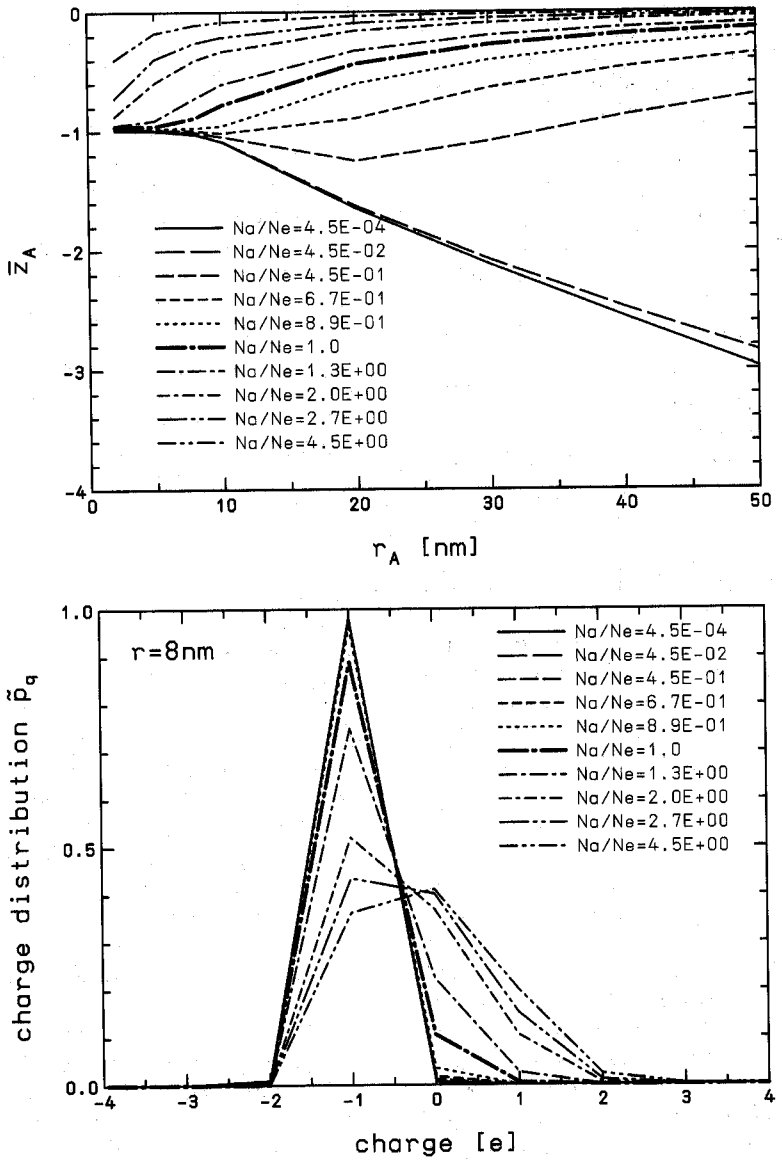

Fig. 4. Upper panel: Mean aerosol charge, $\bar{z}_A = Z_A/N_A$, as a function of aerosol radius, r_A, for various values of N_A/N_e (N_A = aerosol number density; $N_e = \sqrt{Q/\alpha}$ = number density of free electrons). Lower panel: Normalized charge distribution $\tilde{P}_q = 1/N_A \cdot P_q$ of aerosol particles with a radius of 8 nm for various ratios of N_A/N_e.

(e.g. from 1000 to 2000/cm^3 for $\alpha = 10^{-5}$ cm^3/s). This change from ion depletions at low recombination coefficients to ion enhancements at rather large recombination coefficients is caused by a change in the dominant physical process determining the positive ion number density: While for small recombination coefficients the ion number density is controlled by the capture by aerosol particles (thus resulting in a depletion) it is determined by the recombination with electrons in the case of rather large recombination coefficients. Since the electrons are depleted less recombinations occur and the ion densities are enhanced. We note that the results of Reid (1990) and Jensen and Thomas (1991), namely that the positive ion number densities are more or less undisturbed, is only true for their particular choice of $Q = 10/\text{cm}^3\text{s}$ and $\alpha = 10^{-6}$ cm^3/s.

Concerning the aerosol particles we note that most of them are singly negatively charged since each particle on average has captured one electron. The capture of positive ions is negligible due to their low mobility compared to electrons. Charge neutrality is mainly maintained by positive ions and

Table 1
Coefficients for dissociative recombination reactions of positive ions and electrons. The coefficients are given for a temperature of 150 K. The values have been calculated from the results stated in the references applying a theoretically expected temperature dependence of $1/\sqrt{T}$ (Bates, 1950)

Reaction	$\alpha(150\,\mathrm{K})$ ($\mathrm{cm^3/s}$)	Ref.
$O_2^+ + e^-$	$2.7 \cdot 10^{-7}$	Johnson (1981)
$NO^+ + e^-$	$5.9 \cdot 10^{-7}$	Johnson (1981)
$H_3O^+ + e^-$	$1.9 \cdot 10^{-6}$	Leu et al. (1973)
$H^+(H_2O)_2 + e^-$	$3.7 \cdot 10^{-6}$	Leu et al. (1973)
$H^+(H_2O)_3 + e^-$	$5.3 \cdot 10^{-6}$	Leu et al. (1973)
$H^+(H_2O)_4 + e^-$	$6.9 \cdot 10^{-6}$	Leu et al. (1973)
$H^+(H_2O)_5 + e^-$	$7.0 \cdot 10^{-6}$	Leu et al. (1973)
$H^+(H_2O)_6 + e^-$	$8.8 \cdot 10^{-6}$	Leu et al. (1973)
$H^+(H_2O)_7 + e^-$	$1.2 \cdot 10^{-5}$	Leu et al. (1973)

singly negatively charged aerosol particles. This statement is basically independent of α.

In the NLC case (lower panel in Fig. 5) the situation is similar to the PMSE case described above, but the disturbances in the electron and ion number densities are less pronounced and the majority of the aerosol particles is three times negatively charged. Charge neutrality is mainly maintained by electrons and positive ions.

2.3.3. *Varying Q, α, r_A, and N_A*

In order to achieve more general results we have analyzed the dependence of the aerosol plasma interaction on all four parameters, namely Q, α, r_A, and N_A. The results of these calculations are shown in Fig. 6 where relative electron and ion number density disturbances, Δn_e and Δn_i are shown as a function of aerosol number density and radius for various productions rates Q (0.01 to $1000/\mathrm{cm^3\,s}$) and various recombination coefficients α (10^{-7}–10^{-5} $\mathrm{cm^3/s}$). We have used a colour code to distinguish between electron depletions (blue lines), positive ion depletions (red lines), and positive ion enhancements (green lines). Undisturbed positive ions are indicated by a black line.

As can be seen from Fig. 6 electron depletions are nearly always present, i.e., for all combinations of production rates Q, recombination coefficients α, aerosol radii r_A, and aerosol number densities N_A. The electron depletion becomes negligible, say less than 10%, only in case that far more free electrons than aerosol particles exist. Concerning the overall dependence on r_A and N_A, the disturbance increases with increasing aerosol radius and number density.

For fixed α, r_A, and N_A the relative electron disturbance becomes smaller with increasing Q since the free background electron density increases but the absolute number of captured electrons stays more or less the same. Thus, if the production rate Q is small only few aerosol particles are needed to scavenge a major part of the electrons, thus to create a large biteout of say −90%. For moderate production rates (e.g. $Q = 10/\mathrm{cm^3 s}$) a deep biteout is created for a large population of small particles—in agreement with earlier findings of Jensen and Thomas (1991) and Reid (1990)—or for a moderate number of larger particles (e.g., $400/\mathrm{cm^3}$ of radius 50 nm). If the production rate is large ($1000/\mathrm{cm^3 s}$) many large particles are required to produce a significant electron depletion. However, the aerosol size and number densities are limited to a certain extent by the amount of water vapor present in the aerosol particles which should not exceed a reasonable upper limit of approximately 10 $\mathrm{ppm_v}$ (purple lines).

For fixed Q, r_A, and N_A the relative electron depletion varies only little with the recombination coefficient, thus with the positive ion composition. This expresses the fact that the recombination of electrons with aerosol particles is generally more efficient than the recombination with positive ions because the bigger size of the aerosol particles compared to the positive ions results in a much larger (geometric) cross section for the aerosol-electron interaction than for the positive ion–electron interaction.

Again, the dependence of relative positive ion disturbances on the plasma and aerosol parameters is more complex. We start our discussion by considering the line of undisturbed positive ion number densities with varying Q and α. Note that to the right of this isoline, thus for larger particles, ion densities are depleted while for smaller particles ion densities are enhanced compared to the undisturbed profile. The isoline of undisturbed positive ion densities shifts towards larger radii both for increasing Q and increasing α. This implies that for a given particle radius and number density a positive ion density depletion (red lines in Fig. 6) is more likely to be observed under low production conditions (i.e., for large solar zenith angles and low geomagnetic activity).

Independent of radius and number density an ion depletion rather than an enhancement will always occur if the recombination coefficient is small (say, $\alpha = 10^{-7}$ $\mathrm{cm^3/s}$) which is the case if molecular rather than cluster ions prevail. If the recombination coefficient is large (i.e., cluster ions prevail) an ion density depletion will be observed only if both the particle radius and number densities are sufficiently large. Again, the allowed combinations of r_A and N_A are limited by the amount of water vapor present in the aerosol particles which should not exceed say 10 $\mathrm{ppm_v}$. Significant positive ion enhancements (green lines in Fig. 6) are found under moderate to rather low production conditions and are more likely if the recombination coefficient is large.

For an aerosol population representative of NLC conditions (e.g., $r_A = 50$ nm and $N_A = 100/\mathrm{cm^3}$) the ion density will be depleted unless the recombination coefficient is large and, at the same time, the production rate is moderate or large. This leads to the conclusion that if an ion enhancement is observed in the vicinity of noctilucent clouds very large recombination coefficients must have existed indicating the presence of large positive cluster ions (see Table 1).

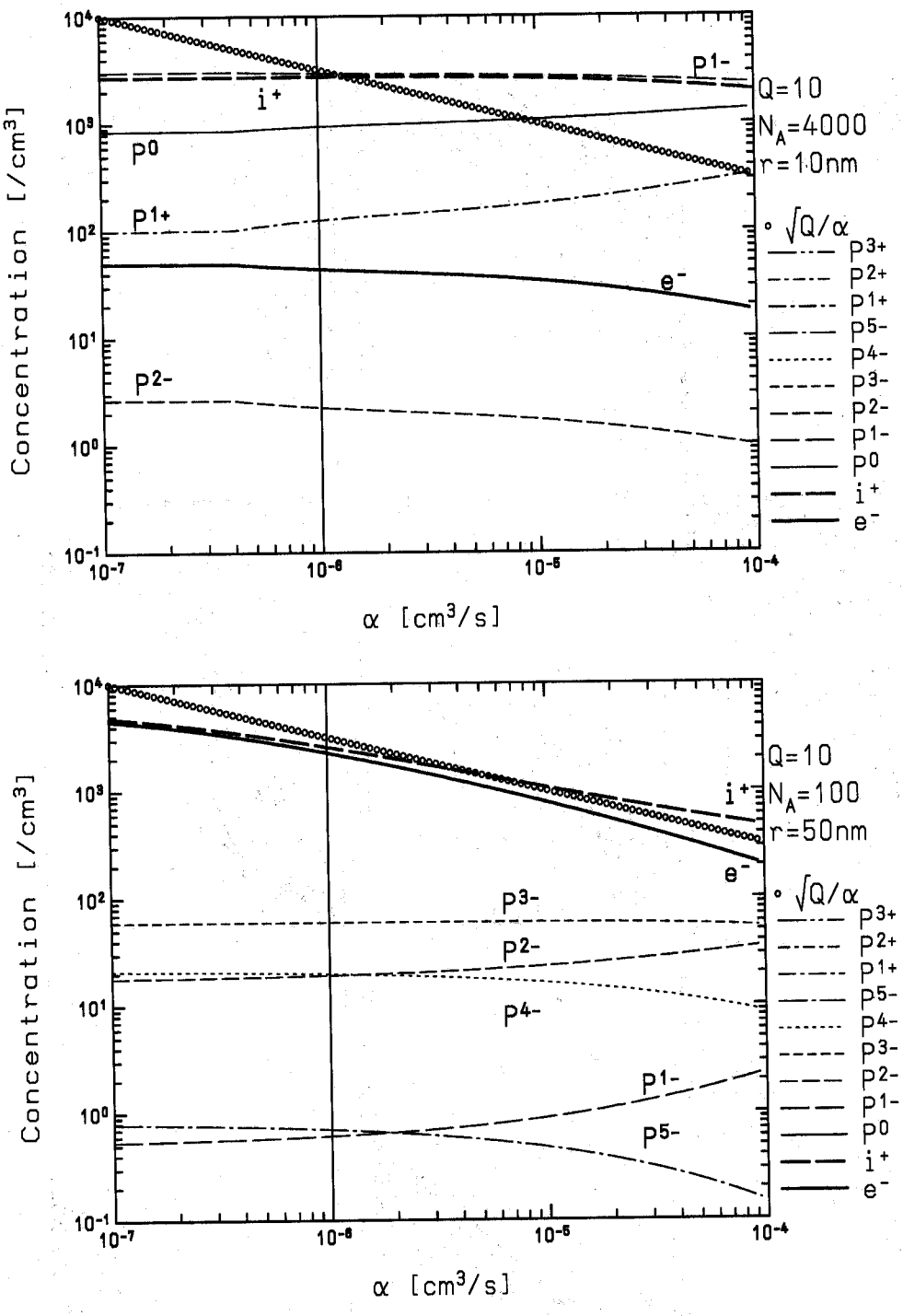

Fig. 5. Upper panel: concentration of charged species as a function of the recombination coefficient. The calculations were performed assuming aerosols with a radius of 10 nm and a number density of 4000/cm^3, and an electron–ion pair production rate of 10/cm^{3}s. Lower panel: same as upper panel but for an aerosol radius of 50 nm and a number density of 100/cm^3. Thick solid line shows the electron concentration, a thick dashed line shows the ions and the thin lines show differently charged aerosol particles labeled $P^{n+/-}$ for n times positively/negatively charged particles. In addition the undisturbed plasma densities $\sqrt{Q/\alpha}$ are marked by large dots.

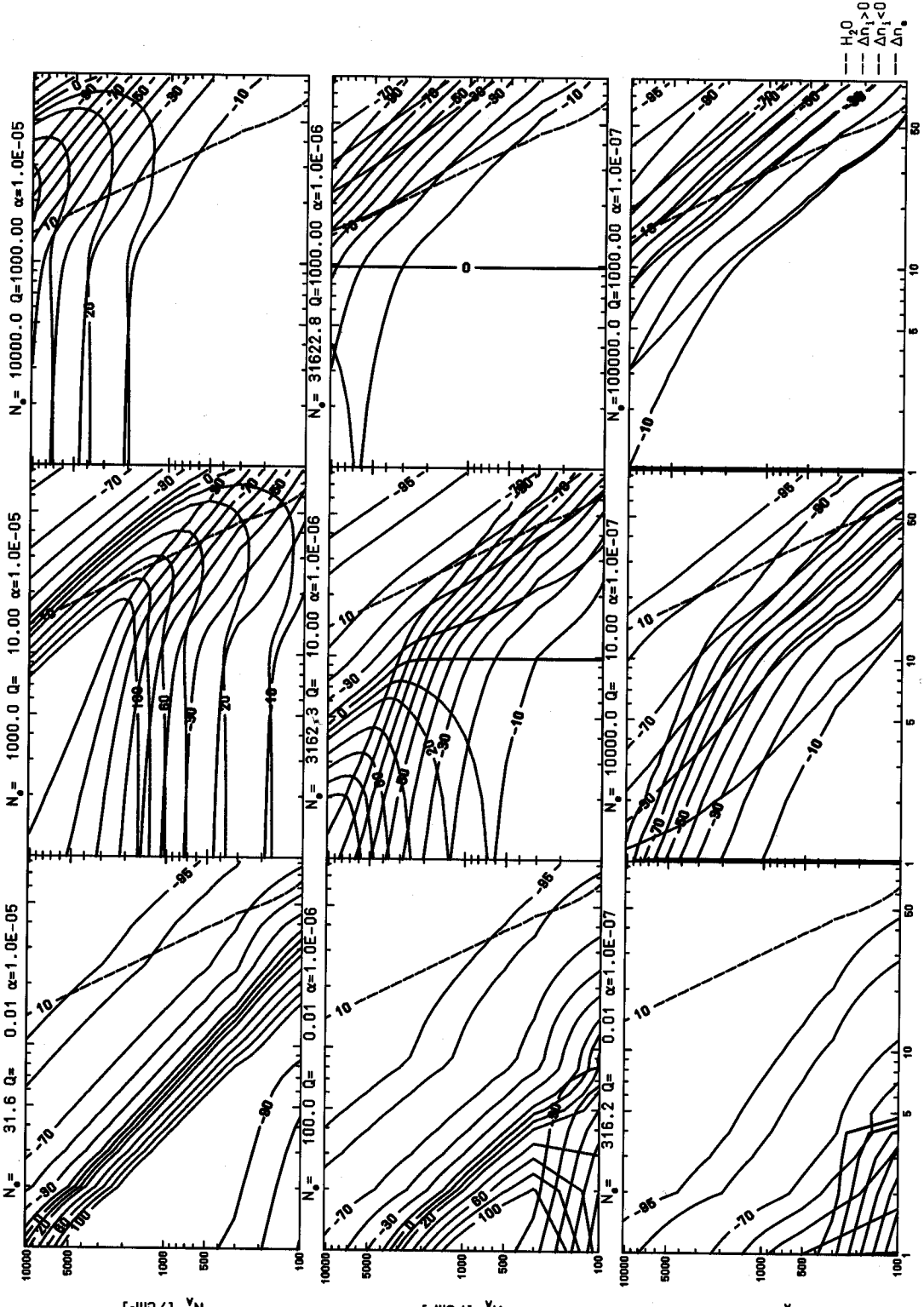

Fig. 6. Contour plots showing the dependence of relative electron and positive ion disturbances on the aerosol radius and number density. In the rows Q has been varied between 0.01, 10, and 1000/cm^{3}s and in the columns α has been varied between 10^{-7}, 10^{-6}, 10^{-5}cm^3/s. Electron depletions are plotted as blue lines, positive ion depletions as red lines, and positive ion enhancements as green lines. An equivalent water vapor content of 10 ppm$_v$ is indicated by a purple line.

For an aerosol population representative of PMSE conditions (e.g., $r_A = 10$ nm and $N_A = 4000/cm^3$) the ion density will be depleted unless the recombination coefficient is large and, at the same time, the production rate is moderate or large. This leads to the conclusion that if an ion enhancement is observed in the vicinity of PMSE small recombination coefficients must have existed which is an indication of the presence of molecular ions.

It is important to note that by varying the background plasma situation and the particle properties nearly all combinations of electron biteouts, ion biteouts and ion enhancements can be created. However, it is not possible to create an electron enhancement. Therefore, the fact that electron enhancements have been observed (Blix, 1999) is a strong indication of an additional charging mechanism which is responsible for a release of electrons from the aerosols, e.g. by the photoelectrical effect (e.g., Rapp and Lübken, 1999).

3. Summary

Revisiting the topic of aerosol charging in the upper summer mesosphere we have demonstrated that the interaction between aerosol particles on the one hand and the background plasma on the other hand is a complicated function of the aerosol radius, the aerosol number density, the ionization rate, and the recombination coefficient. We have demonstrated that the background plasma parameters Q and α show a large natural variability: The ionization rate can vary between values as low as $10^{-3}/cm^3s$ and as large as several $1000/cm^3s$. The recombination coefficient can vary at least between 10^{-7} and $10^{-5}cm^3/s$. This large variability of Q and α has to be taken into account when analyzing plasma disturbances in terms of aerosol charging.

For known Q and α we have shown that in most cases the aerosol radius and number density can be deduced from measurements of electron and positive ion number density. The aerosol particles leave an individual fingerprint in the background plasma profiles.

Concerning the influence of Q, small ionization rates result in a small amount of free electrons and positive ions such that for a sufficient large number of aerosol particles deep biteouts in both electrons and positive ions occur resulting in a net zero particle charge. In this case all electrons and positive ions have been captured by the aerosol particles such that as many aerosol particles carry negative and positive charges. For all other conditions the particles will be negatively charged due to the much higher mobility of electrons compared to positive ions.

The dissociative recombination coefficient α does not show any distinct influence on the electron disturbance. This expresses the fact that electron–aerosol recombination is much more efficient than electron-positive ion recombination due to the large size of the aerosol particles.

In case of positive ions both depletions and enhancements can occur depending on whether the capture by aerosol particles (resulting in a depletion) or the recombination with the depleted electrons (resulting in an enhancement) determines the positive ion number density. Positive ion depletions are most likely observed for low ionization rates. If Q is sufficiently small there are several scenarios which can lead to a distinct biteout. Introducing the constraint given by the maximum of water in the aerosol particles leads to the most probable scenarios of either many small particles ($N_A \gg 10^4/cm^3$, $r_A \approx 1$ nm) or a few large particles ($N_A \approx 100/cm^3$, $r_A \approx 40$ nm). Positive ion number density enhancements can occur for both many small and fewer large particles, but the recombination coefficient has to be sufficiently high ($\approx 10^5$ cm^3/s) appropriate for large cluster ions.

Finally we emphasize that electron number densities cannot be enhanced by any of the combinations of parameters discussed above. To get a surplus of electrons requires an additional physical mechanism to release electrons from the aerosols, for example photo emission.

References

Bates, D.R., 1950. Dissociative recombination. Physical Review 78, 492–493.

Björn, L.G., Arnold, F., 1981. Mass spectrometric detection of precondensation nuclei at the arctic summer mesopause. Geophysical Research Letters 11, 1167–1170.

Blix, T.A., 1999. The importance of charged aerosols in the polar mesosphere in connection with noctilucent clouds and polar mesosphere summer echoes. Advances in Space Research 24 (12), 1645–1654.

Cho, J.Y.N., Hall, T.M., Kelley, M.C., 1992. On the role of charged aerosols in polar mesosphere summer echoes. Journal of Geophysical Research 97, 875–886.

Ecklund, W.L., Balsley, B., 1981. Long-term observations of the arctic mesosphere with the MST radar at Poker Flat, Alaska. Journal of Geophysical Research 86, 7775–7780.

Friedrich, M., Torkar, K.M., 1988. Empirical transition heights of cluster ions. Advances in Space Research 8, 235–238.

Friedrich, M., Torkar, K.M., 1995. Typical behaviour of the high latitude lower ionosphere. Advances in Space Research 16, 73–81.

Garcia, R.R., Solomon, S., 1994. A new numerical model of the middle atmosphere: 2. ozone and related species. Journal of Geophysical Research 99, 12,937–12,951.

Hesstvedt, E., 1961. Note on the nature of noctilucent clouds. Journal of Geophysical Research 66, 1985–1987.

Inhester, B., Klostermeyer, J., Lübken, F.-J., von Zahn, U., 1994. Evidence for ice clouds causing polar mesospheric summer echoes. Journal of Geophysical Research 99, 20,937–20,954.

Jensen, E., Thomas, G.E., 1991. Charging of mesospheric particles: implications of electron density and particle coagulation. Journal of Geophysical Research 96, 18,603–18,615.

Johannessen, A., Krankowsky, D., 1972. Positive ion composition measurement in the upper mesosphere and lower thermosphere at a high latitude during summer. Journal of Geophysical Research 77, 2888–2901.

Johnson, R., 1981. Microwave afterglow measurements of the dissociative recombination of molecular ions with electrons. International Journal of Mass Spectrometry and Ion Processes 81, 67–84.

Kelley, M.C., Farley, D.T., Röttger, J., 1987. The effect of cluster ions on anomalous VHF backscatter from the summer polar mesosphere. Geophysical Research Letters 14, 1031–1034.

Klostermeyer, J., 1997. A height- and time-dependent model of polar mesosphere summer echoes. Journal of Geophysical Research 102, 6715–6727.

Kopp, E., Eberhardt, P., Herrmann, U., Björn, L., 1985. Positive ion composition of the high latitude summer D-region with noctilucent clouds. Journal of Geophysical Research 90, 13,041–13,051.

Leu, M., Biondi, M., Johnson, R., 1973. Measurements of the recombination of electrons with $H_3O^+(H_2O)_n$ series ions. Physical Review A 7, 292–298.

Lübken, F.-J., Rapp, M., 2001. Modelling of particle charging in the polar summer mesosphere: Part 2—application to measurements. Journal of Atmospheric and Solar Terrestrial Physics, 2001, 63, 771–780.

Mitra, A.P., 1981. Chemistry of middle atmospheric ionization—a review. Journal of Atmospheric and Terrestrial Physics 43, 737–752.

Natanson, G.L., 1960. On the theory of the charging of amicroscopic aerosol particles as a result of capture of gas ions. Sov. Phys. Tech. Phys. (English transl.) 5, 538–551.

Nussbaumer, V., Fricke, K.-H., Langer, M., Singer, W., von Zahn, U., 1996. First simultaneous and common-volume observations of NLC and PMSE by lidar and radar. Journal of Geophysical Research 101, 19161–19167.

Parthasarathy, R., 1976. Mesopause dust as a sink for ionization. Journal of Geophysical Research 81, 2392–2396.

Pedersen, A., Troim, J., Kane, J., 1969. Rocket measurement showing removal of electrons above the mesopause in summer at high latitudes. Planetary and Space Science 18, 945–947.

Rapp, M., 2000. Capture rates of electrons and positive ions by mesospheric aerosol particles. Journal of Aerosol Science 31, 1367–1369.

Rapp, M., Lübken, F.-J., 1999. Modelling of positively charged aerosols in the polar summer mesopause region. Earth, Planets and Space 51, 799–807.

Reid, G.C., 1990. Ice particles and electron "bite-outs" at the summer polar mesopause. Journal of Geophysical Research 95, 13,891–13,896.

Reid, G.C., 1997. On the influence of electrostatic charging on coagualation of dust and ice particles in the upper mesosphere. Geophysical Research Letters 24, 1095–1098.

Seele, C., Hartogh, P., 1999. Water vapor of the polar middle atmosphere: annual variation and summer mesosphere conditions as observed by ground-based microwave spectroscopy. Geophysical Research Letters 26, 1517–1520.

Thomas, L., Bowman, M.R., 1985. Model studies of the D-region negative-ion composition during day-time and night-time. Journal of Atmospheric and Terrestrial Physics 47, 547–556.

Turco, R.P., Toon, O.B., Whitten, R.C., Keesee, R.G., Hollenbach, D., 1982. Noctilucent clouds: simulation studies of their genesis, properties and global influences. Planetary and Space Science 3, 1147–1181.

von Cossart, G., Fiedler, J., von Zahn, U., 1999. Size distributions of nlc particles as determined from 3-color observations of nlc by ground-based lidar. Geophysical Research Letters 26, 1513–1516.

von Zahn, U., Bremer, J., 1999. Simultaneous and common-volume observations of noctilucent clouds and polar mesosphere summer echoes. Geophysical Research Letters 26, 1521–1524.